AGU PUBLICATIONS

Geophysical Research Letters

RESEARCH LETTER
10.1002/2017GL074062

Key Points:
- New models for complex landslide emplacement mechanism shed new light on generation mechanisms
- Retrogressive landslide models explain why two giant landslides produce very different tsunamis
- Slow retrogression explains that one of the world's largest landslides produced a small tsunami

Supporting Information:
- Figure S1
- Figure S2
- Figure S2
- Figure S4
- Figure S5
- Table S1
- Supporting Information S1

Correspondence to:
F. Løvholt,
finn.lovholt@ngi.no

Citation:
Løvholt, F., S. Bondevik, J. S. Laberg, J. Kim, and N. Boylan (2017), Some giant submarine landslides do not produce large tsunamis, *Geophys. Res. Lett.*, *44*, doi:10.1002/2017GL074062.

Received 5 MAY 2017
Accepted 1 AUG 2017
Accepted article online 7 AUG 2017

©2017. The Authors.
This is an open access article under the terms of the Creative Commons Attribution-NonCommercial-NoDerivs License, which permits use and distribution in any medium, provided the original work is properly cited, the use is non-commercial and no modifications or adaptations are made.

Some giant submarine landslides do not produce large tsunamis

Finn Løvholt[1], Stein Bondevik[2,3], Jan Sverre Laberg[3], Jihwan Kim[1,4], and Noel Boylan[5]

[1]Norwegian Geotechnical Institute, Oslo, Norway, [2]Western Norway University of Applied Sciences, Institute of Natural Science, Sogndal, Norway, [3]Department of Geosciences, University of Tromsø-the Arctic University of Norway, Tromsø, Norway, [4]Department of Mathematics, University of Oslo, Oslo, Norway, [5]Norwegian Geotechnical Institute, Perth, Western Australia, Australia

Abstract Landslides are the second most important cause of tsunamis after earthquakes, and their potential for generating large tsunamis depend on the slide process. Among the world's largest submarine landslides is the Storegga Slide that generated a large tsunami over an ocean-wide scale, while no traces of a tsunami generated from the similar and nearby Trænadjupet Slide have been found. Previous models for such landslide tsunamis have not been able to capture the complexity of the landslide processes and are at odds with geotechnical and geomorphological data that reveal retrogressive landslide development. The tsunami generation from these massive events are here modeled with new methods that incorporate complex retrogressive slide motion. We show that the tsunamigenic strength is closely related to the retrogressive development and explain, for the first time, why similar giant landslides can produce very different tsunamis, sometimes smaller than anticipated. Because these slide mechanisms are common for submarine landslides, modeling procedures for dealing with their associated tsunamis should be revised.

Plain Language Summary We here study how some of the largest landslides that are observed on the planet may generate destructive tsunamis. The cases of interest are two landslides, named Storegga and Trænadjupet, which occurred about 8000 and 4000 ago below the sea offshore Norway. Their surface areas are similar to the area of Scotland. Surprisingly, only one of these two enormous landslides, Storegga, was known to generate a destructive tsunami. Here we use computer simulations to explain why the other landslide, Trænadjupet, did not produce a a large wave. The computer simulations revealed that differences in the dynamics of the two landslides led to very different tsunamis. This has broader implications on our understanding of how massive submarine landslide generate tsunamis and shows that we need better models to explain why apparently similar landslides generate tsunamis of very different size.

1. Introduction

Landslides are the second most important cause of tsunamis after earthquakes, but their potential to generate ocean-wide catastrophic tsunamis is not well understood and limited to the study of a handful of well-documented events [*Masson et al.*, 2006; *Tappin*, 2010; *Harbitz et al.*, 2014]. The destruction of the Fukushima Daishi nuclear reactor [*Synolakis and Kanoglu*, 2015] in 2011 sets their hazard toward critical facilities sharply into focus. The type of landslide failure and flow process, as well as velocity, acceleration, and volume determine the tsunamigenic strength [*Løvholt et al.*, 2015]. Moreover, landslide tsunamis generally require more sophisticated source or tsunami models than those commonly used for earthquake tsunamis [*Ma et al.*, 2015; *Yavari-Ramshe and Ataie-Ashtiani*, 2016; *Grilli et al.*, 2017]. In this respect, previous models applied for giant submarine landslide tsunamis have fallen short [*Bondevik et al.*, 2005; *Harbitz*, 1992; *Hill et al.*, 2014], as they oversimplify the landslide dynamics and do not incorporate the complex failure process.

While some giant landslides produce large tsunamis, others generate ones that are unexpectedly small. The reason for this difference is due to the slide dynamics, but so far models have been unable to capture this effectively. Tsunami generation from these giant submarine landslides is more complex than those for other landslide types such as rotational slumps [*Lynett et al.*, 2003; *Okal and Synolakis*, 2004; *Tappin et al.*, 2008], for which the generating mechanism is mainly controlled by the initial impulsive landslide motion [*Løvholt et al.*, 2015]. We here use new models to study two major submarine landslides on the Norwegian

continental margin, the 8150 BP Storegga and the ~4500 BP Trænadjupet Slides [*Bryn et al.*, 2005; *Haflidason et al.*, 2004; *Laberg and Vorren*, 2000; *Laberg et al.*, 2002a; *Haflidason et al.*, 2007]. While the Storegga Slide is the only known prehistorical submarine landslide with compelling geological evidence for an ocean-wide catastrophic tsunami [*Bondevik et al.*, 2005, 1997; *Smith et al.*, 2004], such deposits for the giant Trænadjupet Slide are so far absent. To this end, these two landslides comprise unique examples for testing new models and explaining fundamental differences in tsunami generation. First, because of their different onshore tsunami footprints and also because their slide deposits are among the best studied worldwide, which allow us to link the tsunamigenesis to landslide observations.

Examples from different continental margins across the world, including North America and Northern Europe [*Canals et al.*, 2004; *Haflidason et al.*, 2004; *Kvalstad et al.*, 2005; *Masson et al.*, 2006; *Lee*, 2009; *Twichell et al.*, 2009; *Baeten et al.*, 2014] show that large submarine landslides often evolve through retrogressive failure [*Kvalstad et al.*, 2005; *Laberg et al.*, 2002b; *Gauer et al.*, 2005], a process starting somewhere downslope from the headwall area and retreating backward upslope. This retrogressive process is common in clay-rich submarine slopes and is therefore a dominant mechanism in associated landslides worldwide. In this process, landslides often transform into a debris flow and can also develop turbidity currents farther downslope [*Elverhøi et al.*, 2005]. These processes affect how the tsunami is generated, but as noted they have so far not been studied using realistic models.

Here we have tested two new alternative landslide models, a remolding viscoplastic debris flow model, and a retrogressive block model (section 2). These are in turn coupled to tsunami generation and propagation models. In section 3, we present model results using the new models for the 8150 BP Storegga and the ~4500 BP Trænadjupet Slides and compare the simulations with field investigations. In section 4, we discuss the main differences between these two events, and the broader implications of the study, namely, how some massive landslide events may produce tsunamis of only modest size.

2. Methods

2.1. Retrogressive Block Model

The retrogressive block model [*Løvholt et al.*, 2016] is based on the energy balance approach of *Kvalstad et al.* [2005] and assumes that the landslide fails as a continuous sequence of blocks. Each block consists of two triangular subblocks that stay intact during both the failure and slide motion, and a central parallelogram-shaped body subject to simple shear during the failure process (see Figure 1). In addition, the model includes energy dissipation due to plastic shear work along the seabed interface. The initial block geometry is predefined with an initial variable thickness H_0 and a final height of $H_f = H_0 - \Delta H$. The model includes variable topography, variable slide thickness, and hydrodynamic drag terms. Further, a prescribed landslide trajectory and a constant slide width are assumed. The slide thickness is tapered azimuthally using a quadratic function. The model takes into account the energy balance between the kinetic energy E_k (including the block mass m and frontal block speed u), potential energy E_p, the instantaneous plastic internal (E_{int}) and basal plastic friction (E_{base}) energies of the slide, as well as work caused by the hydrodynamic resistance forces due to drag (W_{drag}) and added water mass ($C_m \cdot m$):

$$E_k = \frac{1}{2}(m \cdot (1 + C_m))u^2 = E_p - E_{\text{int}} - E_{\text{base}} - W_{\text{drag}} \tag{1}$$

In this model, the landslide geometry of deformation is predetermined, with an initial block thickness $H_0 = 200$ m, terminal slide thickness $H_f = 100$ m, and a frontal slope of $\beta = 35°$. The landslide speed was to a large degree controlled by the sensitivity of the basal layer S_{base}, this is therefore a free parameter defining the different retrogressive Trænadjupet scenarios. A high basal sensitivity value implies a low basal friction, and vice versa—a low basal sensitivity value implies a higher basal friction. The simulated block motion follows a prescribed path. The retrogressive block model makes use of a series of additional parameters that determine the landslide geometry and soil properties using detailed analytic expressions for E_p, E_{int}, E_{base}, and W_{drag}. These parameters are mainly derived from *Kvalstad et al.* [2005] [see also *Løvholt et al.*, 2016] and are listed in the supporting information.

2.2. Viscoplastic Debris Flow Model Including Remolding

The viscoplastic debris flow model (*BingClaw*) is a depth-averaged Herschel-Bulkley rheological model modified from *Huang and García* [1997] and *Imran et al.* [2001], formulated in an Eulerian system. It solves the mass and momentum balance for a plug (subscript p) and shear layer (subscript s), respectively:

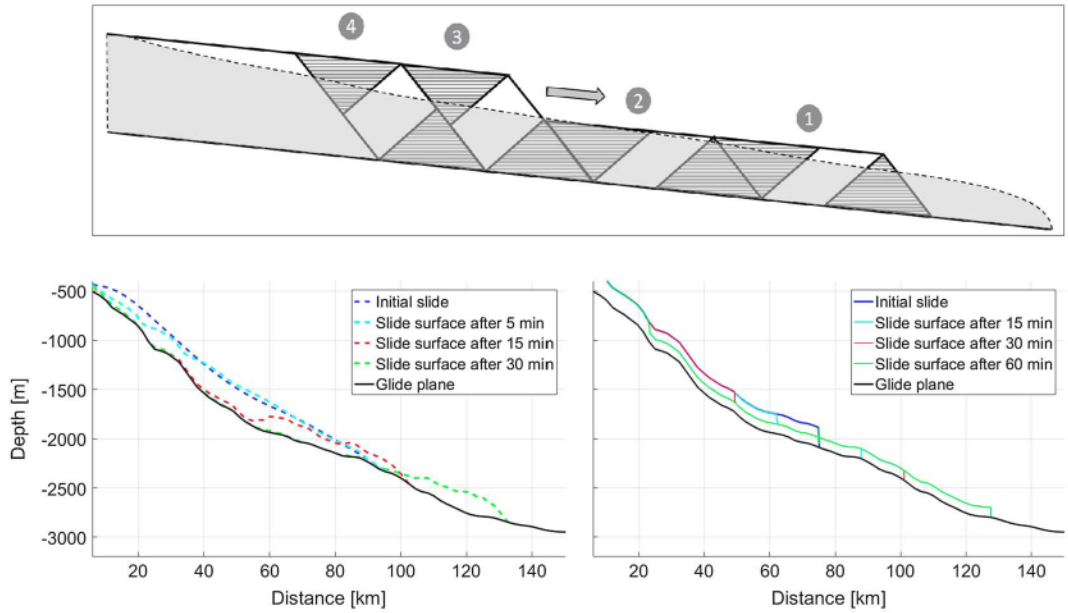

Figure 1. (top) Principle two-dimensional sketch of the failure pattern using a retrogressive block model (triangles and parallelograms) and a remolding debris flow model superimposed in gray. The retrogressive slide blocks fail one by one, blocks 1 and 2 are moving parallel to the slope, blocks 3 and 4 are at rest. The slide material is mobilized more rapidly in the debris flow model, and several "blocks" may fail at the same time. (bottom left) Evolution of the Trænadjupet Slide in the remolding debris flow model. (bottom right) Evolution of the Trænadjupet Slide using the retrogressive block model.

$$\frac{\partial}{\partial t}h + \nabla \cdot \left(h\vec{\mathbf{u}}\right) = 0, \tag{2}$$

and

$$\frac{\partial}{\partial t}\vec{\mathbf{u}}_p + \vec{\mathbf{u}}_p \cdot \nabla\vec{\mathbf{u}}_p + \left(1 - \frac{\rho_w}{\rho_d}\right) g\nabla(h+b) = -\frac{\tau_y \mathrm{sgn}\left(\vec{\mathbf{u}}_p\right)}{h_p \rho_d}, \tag{3}$$

$$\begin{aligned} &\frac{\partial}{\partial t}\left(h\vec{\mathbf{u}}\right) + \left(\left(h_p + \alpha_2 h_s\right)\vec{\mathbf{u}}_p \cdot \nabla\right)\vec{\mathbf{u}}_p \\ &+ \vec{\mathbf{u}}_p\left(\nabla \cdot \left(h_p + \alpha_2 h_s\right)\vec{\mathbf{u}}_p\right) + \left(1 - \frac{\rho_w}{\rho_d}\right) gh\nabla(h+b) \\ &= -\frac{\tau_y \mathrm{sgn}\left(\vec{\mathbf{u}}_p\right)}{\rho_d} - \frac{\tau_y \alpha_3}{\rho_d}\vec{\mathbf{f}}_s. \end{aligned} \tag{4}$$

where $h = h_s + h_p$, is the total landslide thickness over the shear and plug layers, and u_p, v_p, u, and v are plug layer and average velocities in orthogonal directions. The speed of the plug layer and the mean speed is related through the following condition:

$$|\vec{\mathbf{u}}| = \frac{h_p + \alpha_1 h_s}{h}|\vec{\mathbf{u}}_\mathbf{p}|, \tag{5}$$

The water density and debris flow are denoted as ρ_w and ρ_d, respectively, and b represents the undisturbed water depth. This system of equations is solved in three steps: first, by checking that the Earth pressure exceeds the shear strength, then by solving for the terms without friction numerically using a finite volume formulation [*LeVeque*, 2002], and finally, using a fractional step method for the frictional terms. The terms α_1, α_2, and α_3 are functions of the Herschel-Buckley parameters n [see, e.g., *Huang and García*, 1997]. In the present analysis, we set $n = 0.5$. The parameter τ_y is the material yield strength. A validation of BingClaw toward a dambreak problem [*Mangeney et al.*, 2000] is provided in the supporting information

The debris flow model includes remolding. In this way, the material strength is reduced when subjected to shear stresses. The remolding rate Γ is a free parameter, which allows landslide dynamics to mimic complex

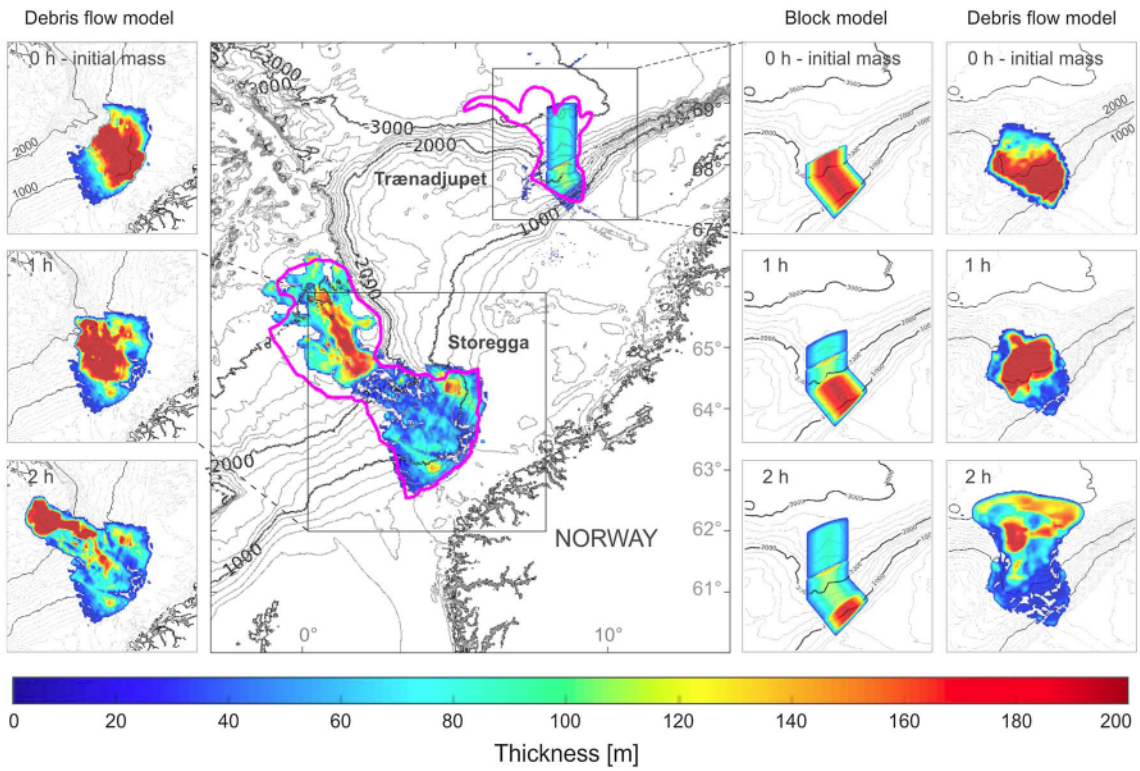

Figure 2. The simulated Storegga and Trænadjupet Slides. Storegga is simulated with the debris flow model; shown are (first column) snapshots at the failure, after 1 h, and after 2 h. Snapshots of the Trænadjupet Slide at the initiation of failure, after 1 h, and after 2 h, (fourth column) using the debris flow model and (third column) using the retrogressive block model (scenario 2). (second column) The final run-out. The observed run-out of the landslide debris are shown as magenta contours.

multistaged failure types such as a retrogressive failure or a top-down failure in a simplified way. When a retrogressive-like failure development is induced, the failure mechanism is different from the one in the retrogressive block model, distributing the failure across a larger portion of the slide mass at the same time, allowing the failure to spread more quickly. Following *De Blasio et al.* [2005], τ_y is subject to remolding according to the equation

$$\tau_y(\gamma) = \tau_{y,\infty} + \left(\tau_{y,0} - \tau_{y,\infty}\right) e^{-\Gamma\gamma}, \tag{6}$$

where $\tau_{y,0}$ and $\tau_{y,\infty}$ are the initial and residual yield strength, respectively, γ is the total shear deformation, and Γ is a dimensionless coefficient. In the present analysis, we use $\tau_{y,0} = 12$ kPa, $\tau_{y,\infty} = 4$ kPa, and $\Gamma = 5 \cdot 10^{-3}$. The term $\vec{\mathbf{f}}_s$ contains quadratic pressure drag and skin friction terms, with coefficients $C_p = 1.0$ and $C_F = 0.01$, respectively. The initial geometries used for this model for Storegga and Trænadjupet are shown in Figure 2.

2.3. Tsunami Models

Tsunami propagation was simulated using depth-averaged shallow water-type models. Initial simulations (see supporting information) demonstrated that dispersive effects had a limited effect on the tsunami propagation, an observation also supported by previous work carried out on voluminous long run-out landslides [*Haugen et al.*, 2005; *Løvholt et al.*, 2005, 2015]. For the tsunami simulations employing the viscoplastic landslide model as the tsunami source, we used a new version of the *GeoClaw* model [*Kim et al.*, 2017] in nonlinear shallow water mode. For the tsunami generation from the retrogressive landslide motion, the numerical *GloBouss* model [*Løvholt et al.*, 2008] was run in linear hydrostatic mode.

The waves are so long that their run-up is effectively captured by the doubling of the tsunami wave amplitude due to coastal reflection. This assumption was used in previous studies of *Bondevik et al.* [2005], *Harbitz* [1992], and *Hill et al.* [2014], the same assumption is used here. That is, we assume that the tsunami elevations at offshore control points placed close to the shoreline to include the amplitude increase due to wave reflection roughly represents the run-up height. The control points are placed in water depths typically ranging from

50 to 100 m, occasionally at as shallow as 10–20 m. We show that this assumption is reasonable by conducting local inundation simulations for two paleotsunami sites (see details in the supporting information, and related data and methods in *Løvholt et al.* [2010] and *Titov et al.* [2013]). These inundation simulations also indicate the typical variability of the run-up that can be expected.

For the Storegga simulations, we used the paleobathymetry of *Hill et al.* [2014], while ETOPO 1 grids were used for the Trænadjupet simulations. For the GloBouss simulations the grids were refined to a resolution of 7.5″ × 15″ before being employed in the tsunami simulations. To correct for nonhydrostatic effects in the tsunami generation due to the short-scale deformations from small retrogressive block lengths, a full potential filter was employed [*Kajiura*, 1963; *Løvholt et al.*, 2015].

3. Results

3.1. New Simulation of the Storegga Slide Tsunami

The Storegga Slide offshore western Norway is among the world's largest landslides, with an estimated slide volume of 2400–3200 km^3 [*Haflidason et al.*, 2004] and a slide area of 95000 km^2. The landslide debris run-out reached about 300 km [*De Blasio et al.*, 2005] on a gentle 1–2° slope, accommodated by the presence of overpressurized base layering [*Bryn et al.*, 2005; *Locat et al.*, 2014]. Geomorphological and geotechnical data conclude that it evolved retrogressively in a single major event [*Kvalstad et al.*, 2005]. The slide deposits below the steep slopes in the slide escarpment show evidence of extensive crushing and disintegration of the retrogressive blocks [*Bryn et al.*, 2005]. Further afield, Storegga produced muddy turbidity currents reaching about 800 km, indicating high slide velocities [*Haflidason et al.*, 2004]. Tsunami deposits from Storegga are found along the Norwegian coastline, in the Faeroe Islands, Shetland, Scotland, and recently in Denmark [*Bondevik et al.*, 2005; *Smith et al.*, 2004; *Fruergaard et al.*, 2015].

The simulation of the Storegga Slide using the debris flow model and a total slide volume of ~3000 km^3 agrees well with observed run-out (see Figure 2). Particularly noticeable is the match of the shape of the landslide debris with observations of landslide lobes [*Haflidason et al.*, 2004], which is only possible due to the model's ability to take into account terrain deflection and shear wetting [*De Blasio et al.*, 2005]. Figure 3 shows that simulated tsunami heights compare well with field observations of sediment run-up in Norway, Faeroe Islands, and offshore Scotland and Denmark, but underestimates the ~20 m run-up observations in Shetland, still clearly improving all previous tsunami hindcasts [*Bondevik et al.*, 2005; *Harbitz*, 1992; *Hill et al.*, 2014].

To achieve the model agreement for the Storegga Slide tsunami, applied values of the ultimate and initial yield strengths and shear wetting rates are in the lower end of both previously assumed and measured values. The slide front accelerated rapidly to a speed of 20 m/s, reaching a maximum frontal speed of 30–35 m/s about 1 h after failure, coming to rest after 5 h. Our simulated slide speeds comply both with previously prescribed block slide speeds in tsunami analysis [*Bondevik et al.*, 2005; *Harbitz*, 1992; *Hill et al.*, 2014], as well as the maximum particle velocity of 60 m/s found in previous simplified run-out simulations of the Storegga Slide [*De Blasio et al.*, 2005].

Simulations using the retrogressive block model as the tsunami source also provided a reasonably good agreement with the Storegga tsunami data, but this model produced larger offsets than the debris flow model between simulations and paleotsunami observations (results not shown). The main tsunami generation took place after the retrogressive process had ended. At this stage, the landslide continued its motion as a solid block. In conclusion, the simulations show that the main tsunami generation of the Storegga Slide took place after the majority of the landslide was mobilized, following a rapid retrogressive process and a high degree of remolding.

3.2. A Small Tsunami From the Giant Trænadjupet Slide?

The ~4500 BP Trænadjupet Slide [*Laberg and Vorren*, 2000] involved a smaller slide velocity than Storegga, and a run-out distance of 100–150 km. Terraces near the upper headwall [see *Laberg et al.*, 2002b, Figure 11] indicate that the event involved retrogressive failure, and most likely it also failed in a single major event. Due to mixing with the older Nyk landslide deposits [*Lindberg et al.*, 2004], precise estimates of its volume do not exist but is smaller than 1000 km^3, and probably closer to 500 km^3. The slide morphology indicates that the landslide deposits located on the abyssal plain are more blocky than corresponding observations of the Storegga Slide [*Laberg et al.*, 2006]. The upper part of the landslide also reveals traces of intact blocks that hint that the slide progression retarded and stopped when the retrogressive slide development progressed

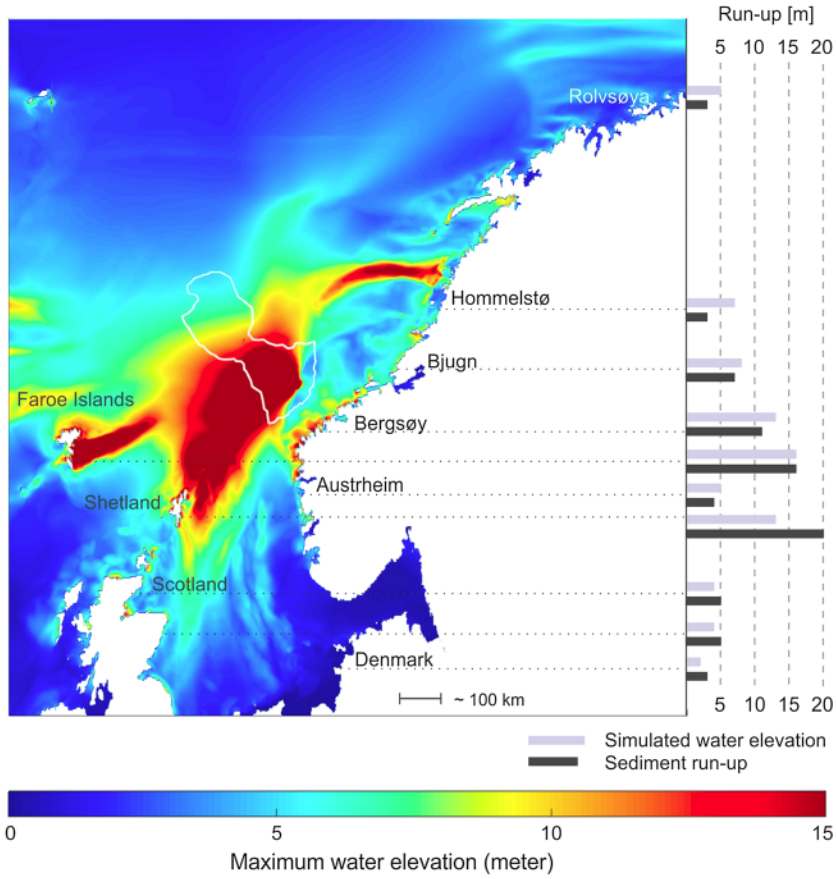

Figure 3. Maximum water elevation for the Storegga Slide tsunami, simulated using the debris flow landslide source. Blue-purple bars show the simulated elevations close to the field sites, black bars show the mean observation heights of sediment run-up [*Smith et al.*, 2004; *Bondevik et al.*, 2005; *Romundset and Bondevik*, 2011; *Fruergaard et al.*, 2015].

to the upper headwall. Finally, we note that Trænadjupet is not associated with extensive turbidity current deposits like those of Storegga. Together, these observations indicate smaller slide velocities than for the Storegga Slide.

We searched for Trænadjupet tsunami deposits in coastal lakes in northern Norway (Figure 4 and supporting information Table S1) but did not find convincing candidates. However, some of the lake basins, marked with a green triangle in Figure 4, have distinct sand laminae(s) in brackish sediments that we interpret to represent a storm surge or a small tsunami. The sand is traced toward the outlet or seaside of the basin, so they must represent a current entering the basins from the sea. But we have not seen erosion or characteristic tsunami facies with rip-up clasts and redeposition, as is typical for Storegga tsunami deposits [*Bondevik et al.*, 1997]. We think the laminaea could represent a small tsunami (less than 3 m run-up) that barely flowed into the lakes, or a major storm surge. A more in depth discussion of the Trænadjupet deposits is given in the supporting information.

The same landslide parameters used for Storegga were employed for the Trænadjupet debris flow simulation, and the simulated landslide thickness and run-out distance agree well with observed landslide deposits [*Laberg and Vorren*, 2000]. The simulated mean frontal velocity using the debris flow model is close to 30 m/s, which is comparable to that of the Storegga Slide debris flow simulation. The snapshots of the landslide in Figure 2 show large initial motions in the upper slope that is reminiscent of a top-down failure. Figure 4 shows that the simulated tsunami induced by the debris flow landslide source produced waves that clearly exceed 2–3 m at many locations. The lack of tsunami deposits show that this scenario is most likely unrealistic for the Trænadjupet Slide based upon our current understanding of the geological evidence. Sufficiently small waves, in agreement with the paucity of tsunami deposits, could only be achieved for scenarios where the landslide could not reach the observed run-out.

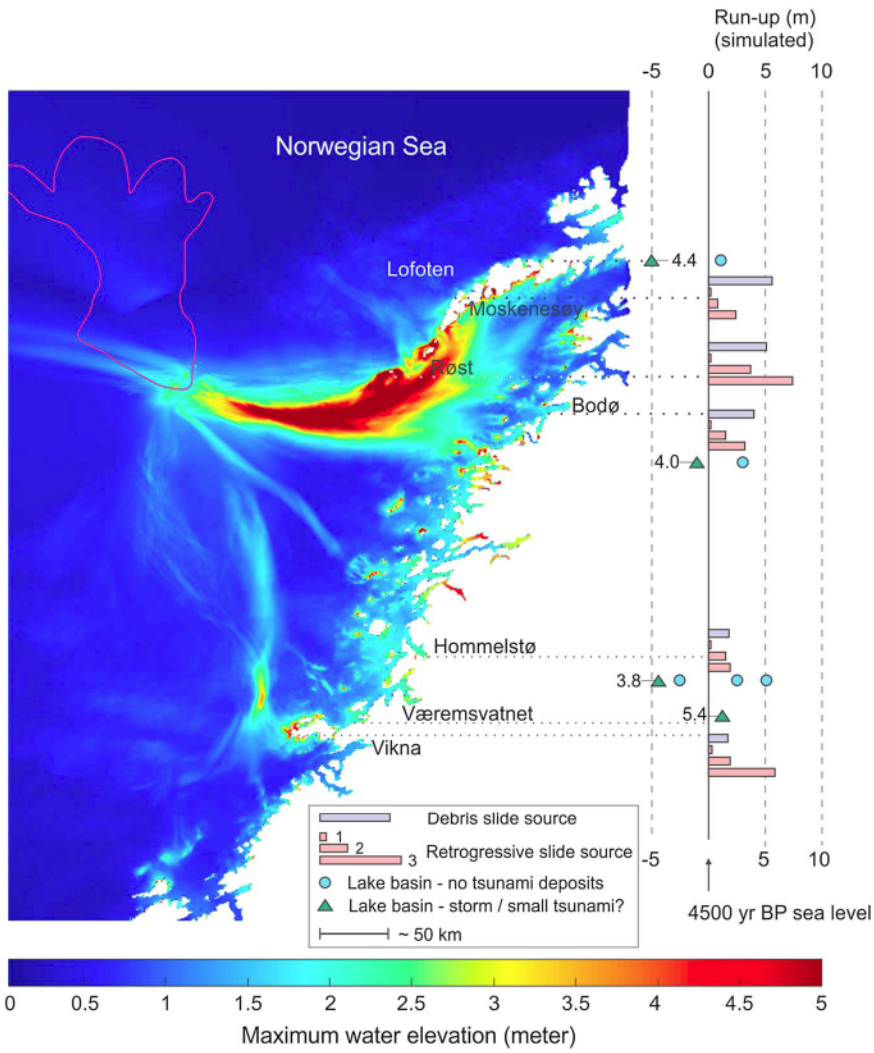

Figure 4. Maximum water elevation for the Trænadjupet Slide tsunami from scenario 2 of the retrogressive landslide model. Blue-purple bars show the simulated near-shore water elevations using the debris flow model as the tsunami source. Pink bars show the simulated elevations using the retrogressive landslide source (scenarios 1–3, from top to bottom). Lake basins with a triangle have unique sand laminae(s) or a zone of coarser sand grains near the brackish/lacustrine boundary. Number next to triangle is age in ka BP of these possible tsunami or storm surge deposits (see supporting information Table S1 for more information). The locations of Vikna and Røst have not been investigated, but represent areas that may be particularly exposed to a Trænadjupet tsunami.

Three scenarios were modeled coupling the retrogressive landslide model to the tsunami model. The first scenario produced the smallest tsunami, with heights less than 0.3 m at the coast. We tuned the base layer sensitivity in this scenario (S=11.75) to terminate the slide motion when the slide retreated to the upper headwall, mobilizing the entire landslide mass (550 km^3). The landslide first accelerates rapidly to reach the maximum velocity of 15 m/s and then decelerates to rest. The slide velocity is therefore low close to the headwall, where the water depth on the continental slope is shallowest. Because the tsunami generation is most efficient for large slide speeds at shallow depth, this process is inefficient at producing a tsunami. The water elevations are less than 1 m offshore, and the height is reduced toward land due to geometric spreading. When the tsunami reaches the potential paleotsunami sites (see Figure 4) the water elevation is below 0.3 m. This scenario represents the weakest possible tsunami source for the Trænadjupet Slide assuming a retrogressive single-event failure. However, this landslide scenario is in agreement with the landslide run-out and evidence at the paleotsunami investigation sites deposits.

In the second and third retrogressive Trænadjupet scenarios we employ slightly larger material sensitivities (S = 14–16), which leads to increased maximum velocities of 17–26 m/s, respectively. In these scenarios the

landslide continues its motion and slides as a single solid block after the retrogressive process has retreated to the headwall, in a top-down motion. Scenarios 2 and 3 therefore result in higher waves. The waves reach more than 5 m in the tsunami generation area as exemplified for scenario 2 in Figure 4. Near the shore, water elevations have a fairly large range of 1–3 m near the field sites. While the scenario 2 simulation gives tsunami heights that are invariably smaller than 2 m at these locations, scenario 3 gives what we consider to be excessive tsunami heights that we should have discovered at the field sites; thus, we think scenario 3 is unlikely. Due to the NW orientation of the slide and focusing and refraction of the tsunami, we find higher waves toward locations such as Vikna (1.9–3.9 m) and Røst (3.7–7.4 m), sites that are not yet investigated for geological evidence. This highlights the point that we cannot rule out that the Trænadjupet event produced a moderately sized tsunami. Comparing all three scenarios, it is clear that the scenarios 2 and 3, involving a top-down block motion following a retrogressive failure, are more tsunamigenic than the pure retrogressive slide (scenario 1).

4. Discussion and Conclusions

The main reason for the difference in tsunami generation for the Storegga and Trænadjupet Slides lies in their different dynamics. The coupled tsunami-debris flow model that produces excellent results for the Storegga Slide, in agreement with both the slide and tsunami deposits, does not work for Trænadjupet, despite the fact that the observed run-out of both slides are well matched in the simulations. This means that in order to quantify the size of the tsunami, it is not sufficient to reproduce the observed landslide run-out in the model. Using the retrogressive block model for the Trænadjupet Slide, we obtain lower slide velocities compatible with the landslide deposits like the thin turbidites in the adjacent deep basins and intact slide blocks in deep water, and the current lack of geological evidence for tsunami inundation. In addition, other factors have played a role resulting in a tsunami or the lack thereof: The Storegga Slide volume is about 5 times larger than Trænadjupet, and a larger portion of it failed in shallower water while moving at greater speed. The distance from the Trænadjupet headwall to shoreline is also about 3 times larger than for Storegga, meaning that the wave was attenuated more before it reached the shoreline. Moreover, the wave directivity due to Trænadjupet is favorable toward locations that we have not yet investigated for tsunami deposits. As a consequence, the new simulations show that a few distant islands along the Norwegian coast might have a record of this event hidden in their geological archives.

In the present paper, we show how differences in failure mechanisms of giant landslides produce very different tsunamis. We further demonstrate that the retrogressive process itself is inefficient in generating tsunamis. This implies that even giant landslides, such as Trænadjupet, may produce tsunamis of only modest size. However, when these voluminous landslides are rapidly transformed into a fast moving debris flow, they are capable of producing a large tsunami like that of Storegga. Many giant landslides across the world's continental margins display retrogressive development, and our examples show that some of them may not produce widespread tsunamis, despite having enormous volumes. While other landslides tend to produce large local waves [*Okal and Synolakis*, 2004], the new results revealed herein show that some landslides, even when exhibiting giant volumes, may be less tsunamigenic than previously thought. The present study shows that their diversity and uncertainty, caused by their very different dynamics and emplacement needs to be reflected in future tsunami hazard assessments.

Acknowledgments
The work has been funded by the Research Council of Norway project Tsunamis induced by large landslides (NFR 231252/F20). We thank Carl Harbitz, Tore Kvalstad, Stefano Lorito, and Carl Fredrik Forsberg, reviewer James Goff, and two anonymous reviewers for their valuable comments that greatly improved the quality of the paper. The source code for viscoplastic debris flow models used to simulate the landslide dynamics is avaible at https://github.com/jhkim2/GRL_BingCLAW. The additional models applied in this study are found in *Kvalstad et al.* [2005], *Løvholt et al.* [2008, 2010], *Titov et al.* [2013], *Løvholt et al.* [2016], and *Kim et al.* [2017].

References

Baeten, N. J., J. S. Laberg, M. Vanneste, C. F. Forsberg, T. J. Kvalstad, M. Forwick, T. O. Vorren, and H. Haflidason (2014), Origin of shallow submarine mass movements and their glide planes—Sedimentological and geotechnical analyses from the continental slope off northern Norway, *J. Geophys. Res. Earth Surf.*, *119*, 2335–2360, doi:10.1002/2013JF003068.

Bondevik, S., J.-I. Svendsen, and J. Mangerud (1997), Tsunami sedimentary facies deposited by the Storegga tsunami in shallow marine basins and coastal lakes, Western Norway, *Sedimentology*, *44*, 1115–1131.

Bondevik, S., F. Løvholt, C. Harbitz, J. Mangerud, A. Dawson, and J. Svendsen (2005), The Storegga slide tsunami comparing field observations with numerical simulations, *Mar. Pet. Geol.*, *22*, 195–208.

Bryn, P., K. Berg, C. Forsberg, A. Solheim, and T. Kvalstad (2005), Explaining the Storegga slide, *Mar. Pet. Geol.*, *22*, 11–19.

Canals, M., et al. (2004), Slope failure dynamics and impacts from seafloor and shallow sub-seafloor geophysical data: Case studies from the COSTA project, *Mar. Geol.*, *213*, 9–72.

De Blasio, F., A. Elverhøi, D. Issler, C. Harbitz, P. Bryn, and R. Lien (2005), On the dynamics of subaqueous clay rich gravity mass flows—The giant Storegga Slide, Norway, *Mar. Pet.Geol.*, *22*, 179–186.

Elverhøi, A., D. Issler, F. De Blasio, T. Ilstad, C. Harbitz, and P. Gauer (2005), Emerging insights into the dynamics of submarine debris flows, *Nat. Hazards Earth Syst. Sci.*, *5*, 633–648.

Fruergaard, M., S. Piasecki, P. Johannessen, N. Noe-Nygaard, T. Andersen, M. Pejrup, and L. Nielsen (2015), Tsunami propagation over a wide, shallow continental shelf caused by the Storegga Slide, southeastern North Sea, Denmark, *Geology*, *43*(12), 1047–1050, doi:10.1130/G37151.1.

Gauer, P., T. Kvalstad, C. Forsberg, P. Bryn, and K. Berg (2005), The last phase of the Storegga Slide: Simulation of retrogressive slide dynamics and comparison with slide-scar morphology, *Mar. Pet. Geol.*, *22*, 171–178.

Grilli, S. T., M. Shelby, O. Kimmoun, G. Dupont, D. Nicolsky, G. Ma, J. T. Kirby, and F. Shi (2017), Numerical simulation of subaerial and submarine landslide generated tsunami waves—Recent advances and future challenges, *Nat. Hazards*, *86*(1), 353–391.

Haflidason, H., H. P. Sejrup, A. Nygård, J. Mienert, P. Bryn, R. Lien, C. F. Forsberg, K. Berg, and D. Masson (2004), The Storegga Slide: Architecture, geometry and slide development, *Mar. Geol.*, *213*(1–4), 201–234, doi:10.1016/j.margeo.2004.10.007. COSTA - Continental Slope Stability.

Haflidason, H., M. de Alvaro, A. Nygard, J. Sejrup, and H. P. Laberg (2007), Holocene sedimentary processes in the Andøya Canyon system, north Norway, *Mar. Geol.*, *246*, 86–104.

Harbitz, C. B. (1992), Model simulations of tsunamis generated by the Storegga Slides, *Mar. Geol.*, *105*, 1–21.

Harbitz, C., F. Løvholt, and H. Bungum (2014), Submarine landslide tsunamis: How extreme and how likely?, *Nat. Hazards*, *72*(3), 1341–1374, doi:10.1007/s11069-013-0681-3.

Haugen, K. B., F. Løvholt, and C. B. Harbitz (2005), Fundamental mechanisms for tsunami generation by submarine mass flows in idealised geometries, *Mar. Pet. Geol.*, *22*, 209–217.

Hill, J., G. Collins, A. Avdis, S. Cramer, and M. Piggot (2014), How does multiscale modelling and inclusion of realistic palaeobathymetry affect numerical simulation of the Storegga Slide tsunami?, *Ocean Modell.*, *83*, 11–25, doi:10.1016/j.ocemod.2014.08.007.

Huang, X., and M. H. García (1997), A perturbation solution for Bingham-plastic mudflows, *J. Hydraul. Eng.*, *123*(11), 986–994, doi:10.1061/(ASCE)0733-9429(1997)123:11(986).

Imran, J., G. Parker, J. Locat, and H. Lee (2001), 1-D numerical model of muddy subaqueous and subaerial debris flows, *J. Hydraul. Eng.*, *127*, 959–968.

Kajiura, K. (1963), The leading wave of a tsunami, *Bull. Earthquake Res. Inst. Univ. Tokyo*, *41*, 535–571.

Kim, J., G. Pedersen, F. Løvholt, and R. Leveque (2017), A Boussinesq type extension of the geoclaw model—A study of wave breaking phenomena applying dispersive long wave models, *Coastal Eng.*, *122*, 75–86.

Kvalstad, T., L. Andresen, C. Forsberg, K. Berg, P. Bryn, and M. Wangen (2005), The Storegga Slide: Evaluation of triggering sources and slide mechanics, *Mar. Pet. Geol.*, *22*, 245–256.

Laberg, J., and T. Vorren (2000), The Trænadjupet Slide, offshore Norway—Morphology, evacuation and triggering mechanisms, *Mar. Geol.*, *171*, 95–114.

Laberg, J., T. Vorren, J. Miener, P. Bryn, and R. Lien (2002a), The Trænadjupet Slide: A large slope failure affecting the continental margin of Norway 4000 years ago, *Geo Mar. Lett.*, *22*, 19–24.

Laberg, J., T. Vorren, J. Miener, D. Evans, B. Lindberg, N. Ottesen, D. adn Kenyon, and S. Henriksen (2002b), Late Quaternary palaeoenvironment and chronology in the Trænadjupet Slide area offshore Norway, *Mar. Geol.*, *188*, 35–60.

Laberg, J., T. Vorren, N. Kenyon, and M. Ivanov (2006), Frequency and triggering mechanisms of submarine landslides of the North Norwegian continental margin, *Norw. J. Geol.*, *86*, 155–161.

Lee, H. (2009), Timing of occurrence of large submarine landslides on the Atlantic Ocean margin, *Mar. Geol.*, *264*, 53–64.

LeVeque, R. (2002), *Finite Volume Methods for Hyperbolic Problems*, vol. 54, 258 pp., Cambridge Univ. Press, Cambridge, U. K., doi:10.1017/CBO9780511791253.

Lindberg, B., J. Laberg, and T. Vorren (2004), The NYK Slide—Morphology, progression, and age of a partly buried submarine slide offshore northern Norway, *Mar. Geol.*, *213*, 277–289.

Locat, J., S. Leroueil, A. Locat, and H. Lee (2014), Weak layers: Their definition and classification from a geotechnical perspective, in *Submarine Mass Movements and Their Consequences*, edited by S. Krastel et al., pp. 3–12, Springer Int., Switzerland.

Løvholt, F., C. B. Harbitz, and K. B. Haugen (2005), A parametric study of tsunamis generated by submarine slides in the Ormen Lange/Storegga area off western Norway, *Mar. Pet. Geol.*, *22*, 219–232.

Løvholt, F., G. Pedersen, and G. Gisler (2008), Oceanic propagation of a potential tsunami from the La Palma Island, *J. Geophys. Res.*, *113*, C09026, doi:10.1029/2007JC004603.

Løvholt, F., G. Pedersen, and S. Glimsdal (2010), Coupling of dispersive tsunami propagation and shallow water coastal response, *Open Oceanogr. J.*, *4*, 71–82, doi:10.2174/1874252101004020071.

Løvholt, F., G. Pedersen, C. B. Harbitz, S. Glimsdal, and J. Kim (2015), On the characteristics of landslide tsunamis, *Philos. Trans. R. Soc. A*, *373*(2053), 20140376, doi:10.1098/rsta.2014.0376.

Løvholt, F., G. Pedersen, and C. B. Harbitz (2016), Tsunami-genesis due to retrogressive landslides on an inclined seabed, in *Submarine Mass Movements and Their Consequences*, edited by G. Lamarche et al., pp. 569–578, Springer Int., Switzerland, doi:10.1007/978-3-319-20979-1_57.

Lynett, P. J., J. C. Borrero, P. L.-F. Liu, and C. E. Synolakis (2003), Field survey and numerical simulations: A review of the 1998 Papua New Guinea Tsunami, *Pure Appl. Geophys.*, *160*, 2119–2146.

Ma, G., J. Kirby, T. Hsu, and F. Shi (2015), A two-layer granular landslide model for tsunami wave generation: Theory and computation, *Ocean Modell.*, *93*, 40–55.

Masson, D., C. Harbitz, R. Wynn, G. Pedersen, and F. Løvholt (2006), Submarine landslides—Processes, triggers and hazard prediction, *Philos. Trans. R. Soc. A.*, *364*, 2009–2039.

Mangeney, A., P. Heinrich, and R. Roche (2000), Analytical solution for testing debris avalanche numerical models, *Pure Appl. Geophys.*, *157*, 1081–1096.

Okal, E. A., and C. E. Synolakis (2004), Source discriminants for near-field tsunamis, *Geophys. J. Int.*, *158*(3), 899–912.

Romundset, A., and S. Bondevik (2011), Propagation of the Storegga tsunami into ice-free lakes along the southern shores of the Barents Sea, *J. Quat. Sci.*, *26*(5), 457–462, doi:10.1002/jqs.1511.

Smith, D., et al. (2004), The Holocene Storegga Slide tsunami in the United Kingdom, *Quat. Sci. Rev.*, *23*(23–24), 2291–2321, doi:10.1016/j.quascirev.2004.04.001.

Synolakis, C., and U. Kanoglu (2015), The Fukushima accident was preventable, *Philos. Trans. R. Soc. A*, *373*, 2014079.

Tappin, D. (2010), Submarine mass failures as tsunami sources—Their climate control, *Phil. Trans. R. Soc. A*, *368*, 2417–2434.

Tappin, D., P. Watts, and S. Grilli (2008), The Papua New Guinea tsunami of 17 July 1998: Anatomy of a catastrophic event, *Nat. Hazards Earth Syst. Sci.*, *8*, 243–266.

Titov, V., U. Kanoglu, and C. Synolakis (2013), Development of most for real-time tsunami forecasting, *J. Waterw. Port Coastal Ocean Eng.*, *142*(6), 03116004, doi:10.1061/(ASCE)WW.1943-5460.0000357.

Twichell, D. C., J. D. Chaytor, U. S. ten Brink, and B. Buczkowski (2009), Morphology of late Quaternary submarine landslides along the U.S. Atlantic continental margin, *Mar. Geol.*, *264*(1–2), 4–15, doi:10.1016/j.margeo.2009.01.009, tsunami hazard along the U.S. Atlantic coast.

Yavari-Ramshe, S., and B. Ataie-Ashtiani (2016), Numerical simulation of subaerial and submarine landslide generated tsunami waves—Recent advances and future challenges, *Landslides*, *13*(6), 1325–1368.